Nuclear Materials and Energy 25 (2020) 100813

Contents lists available at ScienceDirect

Nuclear Materials and Energy

journal homepage: www.elsevier.com/locate/nme

Mechanical and microstructural response of the $Al_{0.5}CoCrFeNi$ high entropy alloy to Si and Ni ion irradiation

M. Aizenshtein [a,*], Z. Ungarish [a], K.B. Woller [c], S. Hayun [b], M.P. Short [d]

[a] Materials Department, NRC-Negev, Beer-Sheva, Israel
[b] Materials Engineering Department, Ben-Gurion University of the Negev, Beer-Sheva, Israel
[c] Plasma Science and Fusion Center, Massachusetts Institute of Technology, Cambridge, MA 02139, USA
[d] Department of Nuclear Science and Engineering, Massachusetts Institute of Technology, Cambridge, MA 02139, USA

ARTICLE INFO

Keywords:
$Al_{0.5}CoCrFeNi$
HEA
Irradiation damage
Nanoindentation

ABSTRACT

The nearly infinite compositional design space of high entropy alloys (HEAs) presents many opportunities to improve performance in extreme environments, particularly for nuclear reactors. The ability of some HEAs to resist high amounts of radiation damage, while well documented, has not yet been fully exploited. We studied the irradiation effect of different ions (Si and Ni) on the microstructure and mechanical properties of the $Al_{0.5}CoCrFeNi$ alloy at its equilibrium state, and of the individual response of each phase to irradiation. The results show a stronger effect of Si ions and differences in response of the ductile FCC (A1) and brittle ordered BCC (B2) phases towards irradiation. This finding highlights the need to further probe unexplored compositional spaces in HEAs, as further optimization is likely to yield further compositional and microstructural stability with practical applications.

1. Introduction

High entropy alloys (HEAs) can possess unique combinations of properties not often observed together such as thermo-mechanical stability at elevated temperatures, high strength, ductility, and corrosion resistance [1–4]. The properties of these HEAs could meet the requirements of structural materials in next-generation nuclear reactors, which will operate in severe environments, at high temperatures, and incur high radiation doses [5,6].

The $Al_xCoCrFeNi$ system has been used as a model system for studying the behavior of HEAs under irradiation. Its structural stability appears to result from the phase(s) of the alloy, which for the case of $Al_xCoCrFeNi$ can be a mixture of FCC and BCC, with the latter playing an important role in hardening the alloy [10]. At equilibrium, the content of each phase depends on the Al fraction (x) [10]. Below $x < 0.5$, the alloy contains a single FCC phase (A1), for $0.5 \leq x < 0.9$, the alloy is mixture of FCC (A1) and ordered BCC (B2) phases, and for $0.9 \leq x \leq 2$ it contains a mixture of ordered and disordered BCC phases (B1 and A2). This equilibrium state could be disturbed by external fields and forces, for example, at high external pressure, Wang et al. [11] studied Al_x-$CoCrFeNi$ ($0 < x < 1.5$) up to ~ 50 GPa and demonstrated that the FCC and BCC phases could transform to HCP. Wang et al. [12] argued that external forces influence kinetics as well. They showed that cold rolling of $Al_{0.5}CoCrFeNi$ led to higher phase transformation rates due to an increase in defect density, which promotes nucleation and growth. Irradiation could accomplish this as well, since it introduces many microstructural defects and in particular can induce radiation induced segregation and formation of non-equilibrium phases.

Yang et al. [7] studied the precipitation behavior of as-cast Al_x-$CoCrFeNi$ alloys (where $x = 0.1, 0.75, 1.5$) irradiated by 3 MeV Au ions up to ~ 40 displacements per atom (DPA) at room temperature. They reported that the $Al_{x=0.1}$ alloy, which exists as a single FCC phase, exhibits improved phase stability under ion irradiation with no precipitates found even at a dose of ~ 43 DPA. On the other hand, the other two multi-phase alloys exhibited significant nanoscale precipitation following irradiation, with precipitation found in both the FCC and the BCC phases. The precipitation occurring in the FCC (A1) phase of the multi-phase $Al_{x=0.75}$ alloy compared to the single-phase FCC (A1) alloy could be explained by slightly different compositions exhibiting very different phase stability. The single FCC phase contains 22.5 and 25.3 at. % Cr and Ni respectively, while the $Al_{x=0.75}$ alloy contains 26.1 at. % of both elements. The slightly higher Cr and Fe content in the FCC phase increases the impact of the high positive Cr-Fe mixing enthalpy to reduce thermodynamic stability and impart a driving force for

* Corresponding author.
E-mail address: aizensht@post.bgu.ac.il (M. Aizenshtein).

https://doi.org/10.1016/j.nme.2020.100813
Received 8 July 2020; Received in revised form 29 August 2020; Accepted 21 September 2020
Available online 22 October 2020

precipitation. Xia et al. [8] studied the same three compositions in the same HEA system, also under Au ion irradiation, at higher DPA (105, 91, and 81 for x = 0.1, 0.75, and 1.5 respectively) at room temperature. In contrast to Yang et al. [7] and although they irradiated their specimens to higher doses, no significant ordering, amorphization, or phase separation of these three alloys were observed. Moreover, a quantitative comparison of the defect cluster sizes in the $Al_{x=0.75}$ and $Al_{x=1.5}$ HEAs reveals that the defect clusters in the disordered FCC (A1) and disordered BCC phase (A2) occur at much smaller sizes with lower frequencies than those in the ordered BCC (B2) phase. This effect may be explained by slower defect mobility in the disordered phase, mechanistically agreeing with one of the proposed mechanism of HEA stability under irradiation [13].

In another study, Xia et al. [9] showed that radiation void swelling in these alloys is significantly lower than conventional nuclear materials (such as 316 stainless steel) at the same irradiation conditions (3 MeV Au ions, up to ~ 65 DPA). Interestingly, swelling in the FCC phase was lower than that in the BCC phase, opposite to the trend in conventional nuclear materials [9].

Irradiation effects in the $Al_xCoCrFeNi$ system have also been studied at elevated temperatures. Yang et al. [14,15] studied the $Al_{0.1}CoCrFeNi$ and $Al_{0.3}CoCrFeNi$ systems under 3 MeV Au ion irradiation up to 650 °C. For the $Al_{0.1}CoCrFeNi$ alloy, they concluded that at ~ 31 peak DPA no phase precipitation took place, while the $Al_{0.3}CoCrFeNi$ alloy exhibited irradiation-induced precipitation of B2 phase at 650 °C due to irradiation enhanced diffusion. Kombaiah et al. [16] irradiated the $Al_{0.12}CoCrFeNi$ alloy with 3 MeV Ni^{+2} ions up to ~ 100 DPA at 500 °C and found that the ordered Ni_3Al phase was formed. The Authors propose that radiation-enhanced non-equilibrium diffusion took phase and also exhibited extensive formation of voids in their study.

In all cases described above, the microstructures of the as-cast alloys exhibit nm-sized secondary phases (FCC or BCC, depending on composition) which inherently include high defect densities. In this work we study the response of the $Al_{0.5}CoCrFeNi$ HEA in its stabilized, equilibrium state to ion irradiation. We irradiated the $Al_{0.5}CoCrFeNi$ alloy with Si and Ni ions, which besides the mass difference, better mimics the influence of transmutation atoms formed under neutron irradiation; Ni represents potential transmutation atoms which exist in the alloy prior to irradiation while Si represents new atoms created by the $Al(n,p^+)Si$ nuclear reaction. We observe that the $Al_{0.5}CoCrFeNi$ HEA contains a mixture of the ductile FCC (A1) phase and the hard, brittle, ordered BCC (B2) phase, constituting a metallic composite with improved mechanical properties compared to previously investigated HEAs in the same compositional system.

2. Experimental

2.1. Sample preparation

The $Al_{0.5}CoCrFeNi$ alloy was prepared by arc melting under ultra-high (99.999%) purity argon atmosphere with a Ti-getter to consume all available oxygen. The purity of raw materials used was higher than 99.9%. The alloy was melted and turned over five times to increase homogeneity, followed by final casting into a 6 mm diameter rod. For heat treatments, samples were cut from the as-cast alloy, wrapped in Ta foil, and sealed in quartz capsules. Then the samples were heat-treated at 900 °C for 7 days and furnace cooled to room temperature.

Samples for SEM characterization were prepared using standard metallographic procedures. For the ion irradiation experiments, samples 6 mm in diameter were polished down using various grits of SiC paper and diamond paste, from 320 grit to 0.25 μm diamond paste. In order to remove surface stresses, the samples were vibratory polished using a pH-neutral colloidal 50 nm silica suspension for 5–6 h. This was performed to remove any cold work from previous polishing steps from the material surfaces to be ion irradiated.

2.2. Ion irradiation

The $Al_{0.5}CoCrFeNi$ samples were irradiated at the Cambridge Laboratory for Accelerator Study of Surfaces (CLASS) at MIT, which houses a 1.7 MV Tandetron accelerator. A first group of samples were irradiated with a defocused 5 MeV Ni^{+3} beam such that the beam current density profile as measured by a National Electrostatics Corporation Beam Profile Monitor was a 2-dimensional Gaussian with a FWHM (full width half maximum) of 7.7 mm. The beam was collimated by an 8 mm diameter aperture. The total fluence used in irradiation 1 was $8.78 \cdot 10^{15}$ Ni/cm^2 averaged across the 8 mm diameter beam-exposed area. Based on SRIM calculations [17] in quick Kinchin-Pease mode [18] using recommended displacement energies from ASTM E521-96 [19], the peak in the damage depth profile for irradiation 1 was 18.7 DPA at a depth of ~ 1.6 μm (Fig. 1a). The temperature of the samples during irradiation 1 remained below 45 °C as measured by a K-type thermocouple mounted inside the sample holder block. The second set of samples was irradiated with a 5 MeV Si^{+3} beam with a FWHM of 11.8 mm to total area-averaged fluence of $1.57 \cdot 10^{16} Si/cm^2$ through the 8 mm diameter aperture. The SRIM calculations for irradiation 2 resulted in peak damage values of 15.3 DPA at a depth of ~ 1.4 μm (Fig. 1b). In irradiation 2, the average temperature of the samples was 113 °C over the course of the ~ 2-hour irradiation with a maximum temperature of 140 °C. Using diffusion coefficients for similar systems [20], diffusion is not expected to take place at these experimental conditions and times beyond the order of a single lattice constant.

2.3. Mechanical property measurement

An Anton Paar NHT^2 nanoindentation tester equipped with a modified Berkovich indenter was used to study the mechanical response of irradiated and unirradiated regions of each sample. Continuous stiffness measurement was used up to a depth of 2 μm, with a loading speed of 5 nm/min, and the maximum load was held for 10 sec. Six nanoindentation measurements were taken both from irradiated and non-irradiated regions. The triangular indentation area measured at a depth of 2 μm was ~ 100 μm^2, which assures a representative measurement of the sample containing both A1 and B2 phases (see Fig. 2 for a typical micrograph showing both phases and their morphologies).

2.4. Microstructural characterization

The structure and composition of the obtained phases were characterized using X-ray diffraction (XRD), High Resolution Scanning Electron Microscopy (HR-SEM), and Transmission Electron Microscopy (TEM). XRD analysis was performed using an Empyrean Alpha 1 diffractometer (Malvern Panalytical Ltd., Royston, UK) with Cu-K_α radiation. XRD spectra were obtained at 40 kV and 30 mA in the 2θ range of 20-120°, with a step size of 0.02° and a scan step time of 1 sec. In addition to phase identification, the XRD data were used to evaluate strain in the irradiated and un-irradiated samples based on the Williamson–Hall method [21]. SEM analysis was performed using a Verios XHR 460L instrument equipped with a Noran Energy Dispersive Spectrometer (EDS) at a 15 kV beam voltage. A 200 kV TEM (JEOL JEM-2100F, Peabody, MA, USA) was used to obtain structural information at the nanoscale, using selected area electron diffraction (SAED). The TEM sample was extracted from the surface of the SEM sample by using a focused ion beam (FIB, Helios G4 UC, Thermo-Fisher Scientific, MA, USA).

3. Results

3.1. Microstructural evolution under irradiation

The microstructure of the unirradiated $Al_{0.5}CoCrFeNi$ alloy heat-treated at 900 °C for 7 days is presented in Fig. 2. Based on Refs.

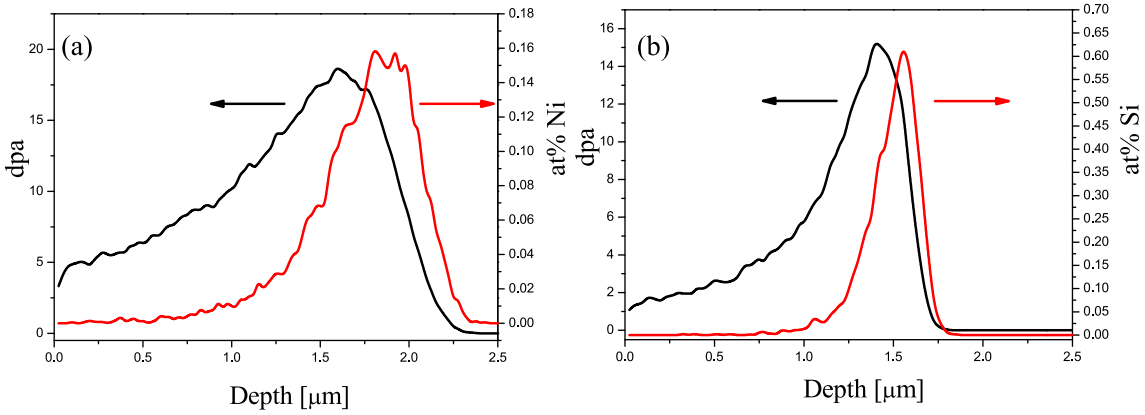

Fig. 1. SRIM calculations of the damage (dpa) and implanted ion profiles for Ni (a) and Si ion irradiation (b).

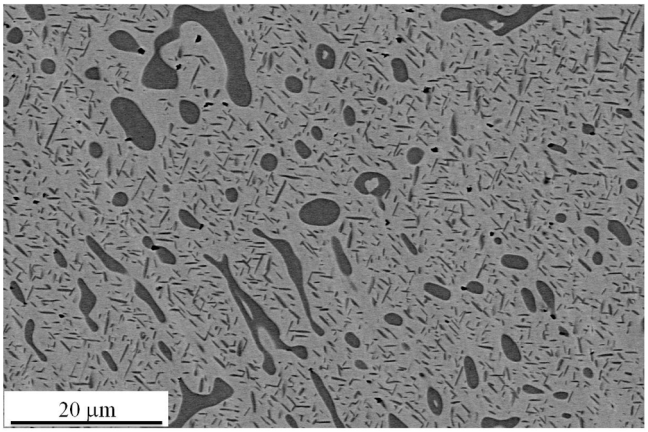

Fig. 2. Backscattered electron microscopy image of the $Al_{0.5}CoCrFeNi$ alloy after heat-treatment at 900 °C for 7 days. Bright area – FCC phase (A1), dark area – ordered BCC (B2).

[22–24] concerning the compositions and morphologies of phases in $Al_xCoCrFeNi$ alloys, the B2 phase is Al- and Ni-rich with a coarse, discontinuous morphology decorating the as-cast A1 phase dendrites (Co–, Cr-, and Fe-rich) and a finer "needle-like" form, which precipitated during heat-treatment, inside the dendrites.

TEM analysis of the Ni- and the Si- ion irradiated samples shown in Figs. 2-3 showed no significant damage (amorphization or voids) detected in either A1or B2 phases, similar to the reported data by Xia et al. [8]. Yet, bright field TEM images imply that the dislocation density increases in the A1 phase of the Ni and Si ion irradiated samples compared to the un-irradiated sample (Fig. 3). In order to verify this observation, the weak beam imaging method was applied (Fig. 4). This method was used in various studies of HEAs, aimed at highlighting dislocations and stacking faults [25–27]. It is seen that the dislocation density increases in the A1 phase when ion irradiation is applied and that the dislocation density is comparatively higher for the Si ion irradiated sample.

3.2. XRD line broadening analysis

Defects and atoms introduced by ion irradiation at ambient temperature are expected to increase strain in materials. The Williamson–Hall method [21] was used in order to evaluate these strains in the FCC and BCC phases, both in the irradiated and un-irradiated conditions. According to this method, the lattice strain (ε) is extracted from the broadening of XRD reflections according to equation (1):

$$\beta cos(\theta) = \frac{K\lambda}{D} + 4 < \varepsilon^2 > sin(\theta) \quad (1)$$

where β is the total width of the reflection, θ is the Bragg angle, K is the Scherrer constant, λ is the X-ray wavelength, and D is the average grain or crystallite size. The slope of the line fitted to $\beta cos(\theta)$ vs. $4sin(\theta)$ is equal to the mean square of the strain. The reflections used for the A1 phase were (111), (200), (220), and (311), while for the B2 phase the (100), (110), (200), (211), and (220) reflections were used. Fig. 5 shows that the strains of the A1 and B2 phases in the un-irradiated sample are similar within the limits of their uncertainties (0.1 ± 0.03 and 0.09 ± 0.01 respectively). After ion irradiation the strain in the B2 phase increased remarkably compared to the un-irradiated state. Furthermore, the impact of Si-ion irradiation on the strain state is markedly higher that than of Ni-ion irradiation. In the case of the A1 phase, irradiation seems to reduce strain. The strains in the Si irradiated material are higher than in the case of Ni irradiated sample, although the difference is rather insignificant.

3.3. Nanoindentation-Measured mechanical properties

Mechanical properties of the irradiated and un-irradiated $Al_{0.5}CoCrFeNi$ alloys were determined by nanoindentation, with six measurements taken from each specimen. The results are presented in Fig. 6. It is seen the hardness of the ion irradiated samples is higher than the un-irradiated samples.

The data acquired could also be used to calculate the integral hardness of the irradiated layer according to the Nix-Gao model [28]:

$$\frac{H}{H_0} = \sqrt{1 + \frac{h^*}{h}} \quad (2)$$

Where H is the nanohardness for a given depth h of indentation, H_0 is the hardness at infinite depth, and h^* is a characteristic length that depends on the indenter tip and tested material. The Nix-Gao plots for the irradiated and un-irradiated materials are presented Fig. 7.

The critical indentation depths, in which the nanoindenter starts measuring the un-irradiated zone in addition to the irradiated volume, are ~ 380 nm for Si ions and ~ 550 nm for Ni ions. These are denoted by the points where the slopes change in Fig. 7, and where hardness drops sharply with increasing depth. This is in agreement with the shallower dpa peak of Si compared to Ni irradiation, as seen in the SRIM calculations (Fig. 1).

The extracted values of H_0 from Fig. 7, are presented in Table 1 (H_0^2 intersects with the Y axis at $h \to \infty$). It is seen that the hardness in the Si and Ni irradiated samples increased by 71% and 34% respectively, compared to the un-irradiated sample.

It could be seen that Si ion irradiation hardens the alloy more than Ni ion irradiation on a per DPA basis, in agreement with the XRD and TEM

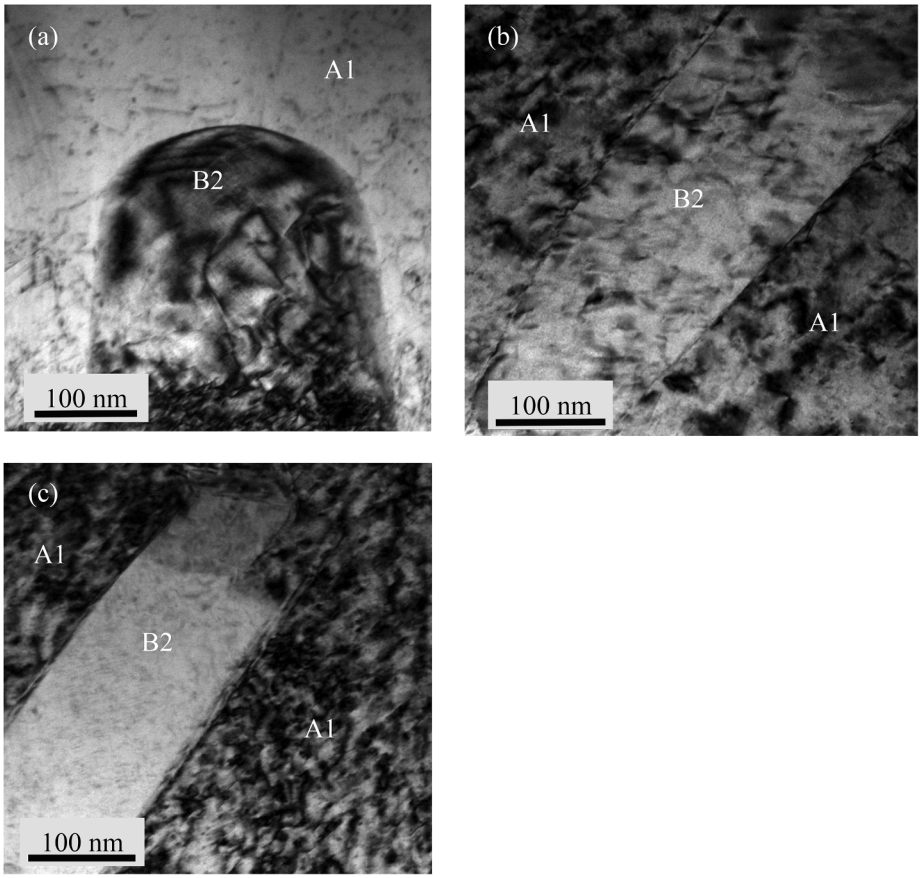

Fig. 3. Bright field TEM images of the $Al_{0.5}$CoCrFeNi alloy after heat-treatment at 900 °C for 1 week. (a) Un-irradiated (b) Ni-ion irradiated alloy (c) Si-ion irradiated alloy.

results presented earlier, which show more change in slope of the XRD patterns and microstructural evolution in the TEM, respectively.

4. Discussion

The potential applicability of HEAs to function in nuclear reactors, either as structural materials for both fission and fusion or for plasma facing components for fusion reactors, hinges upon their ability to maintain their material properties and structural stability under irradiation. Various theories have been proposed to explain the resistance of HEAs to radiation damage, including high chemical complexity [29], high configurational entropy [7], higher defect formation enthalpies [30], high potential energy landscape (PEL) heterogeneity as quantified by migration enthalpy variance [31], and high intrinsic lattice stresses. These theories ultimately hinge upon the frustration of rapid 1D interstitial diffusion [32] or dislocation loop mobility [33], inducing more sluggish 3D diffusion [13] which favors more localized vacancy-interstitial recombination [34] and thus reduces the number of defects surviving radiation damage. The most scientifically interesting conclusion which can be drawn from this paper is that the resistance of Al_xCoCrFeNi HEAs to radiation does not vary monotonically with changing Al composition. Instead it appears we observe an "island of stability", consistent with previous studies, whereby two competing effects which impart radiation damage resistance work together better at the $Al_{x=0.5}$ composition compared to previously investigated $Al_{x=0.1}$ and $Al_{x=0.75}$ ones. In the $Al_{x=0.1}$ case, previously cited effects of PEL heterogeneity, high compositional entropy, and intrinsic lattice strains are all in play to combat radiation defect production and clustering. These are restricted to single-phase, solid-solution effects. In the $Al_{x=0.75}$ case the benefit of interfaces as sinks for radiation damage comes into play. In the case of our $Al_{x=0.5}$ HEA, all are in effect, enhanced by the very fine, high-surface-area morphology of the B2 precipitates formed after heat treatment. We now turn to some of the finer points to discuss, namely evidence that point defects cause proportionally more mechanical property degradation on a per-defect basis, and on mechanisms of damage accumulation and subsequent plastic deformation in the AlCoCrFeNi HEA system.

The nanoindentation results show an increase in hardness of both ion irradiated materials, whereas the effect of Si ions is seen to be stronger than that of the Ni ions on a per-ion basis. It is interesting to understand the different impact of Si and Ni on irradiation hardening and furthermore to understand the hardening mechanism. It should be noted that while Fig. 6 shows lower peak hardness for the Si-irradiated case, the Ni-ion and Si-ion irradiations were conducted to doses of 18.7 DPA and 15.3 DPA, respectively. When scaled to equivalent doses, the peak excess hardening from Si-ion irradiation slightly exceeds that of Ni-ion irradiation. Therefore Si-ions harden the alloy more on a per-ion basis compared to Ni-ions. This is further evidenced by the somewhat increased strain in both phases, observed in Fig. 5, resulting from Si-ion irradiation compared to Ni-ion irradiation. The effect is more pronounced in the B2 needle-like phase than in the A1 FCC phase.

Intrinsic strain is an inherent property of HEAs, and retention of this intrinsic, atomic-level strain after irradiation could be an indicator of radiation damage resistance. According to Refs. [35,36] which sought to generalize characteristic properties of multi-component solid solution systems, an important parameter affecting phase formation in HEAs is the atomic size difference, expressed as the lattice distortion parameter:

$$\delta = \sqrt{\sum_{i=1}^{n} c_i \left(1 - \frac{r_i}{\overline{r_i}}\right)^2} \tag{3}$$

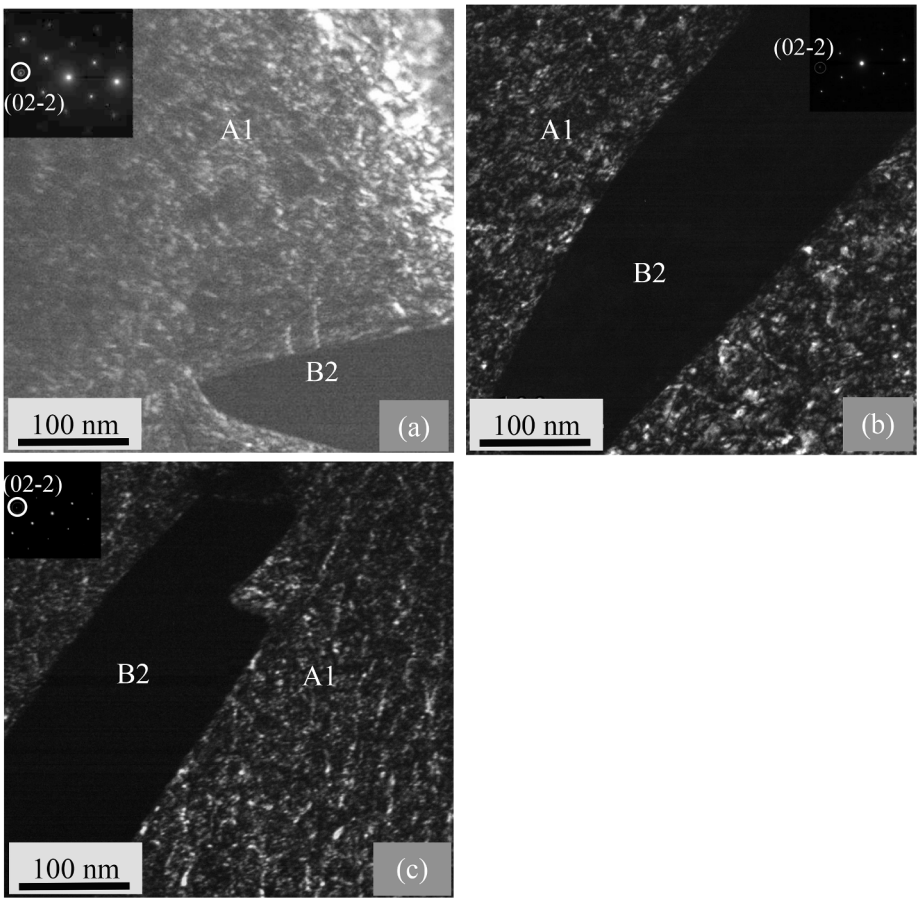

Fig. 4. Weak beam dark-field TEM images. (a) Un-irradiated alloy (b) Ni irradiated alloy (c) Si irradiated alloy.

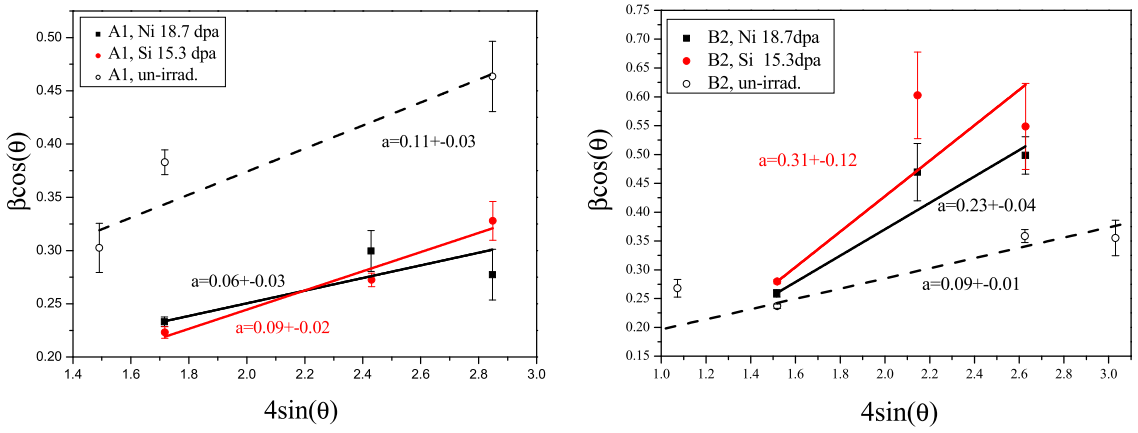

Fig. 5. Williamson-Hall analysis for the A1 and B2 phases observed in the $Al_{0.5}CoCrFeNi$ alloy, for both Ni and Si ion irradiated and un-irradiated conditions (a = slope).

Where c_i is the atom fraction of the i^{th} component, r_i is the atomic radius (143 pm, 125 pm, 129 pm, 126 pm, 125 pm, and 111 pm for Al, Co, Cr, Fe, Ni, and Si respectively [37]), and $\overline{r_i}$ is the alloy's average atom radius, expressed as $\overline{r_i} = \sum_{i=1}^{n} c_i r_i$. The atomic size difference is proportional to the lattice distortion, and a large value of δ implies a large lattice distortion.

The compositions of the A1 and B2 phases in the $Al_{0.5}CoCrFeNi$ alloy after heat-treatment at 900 °C are presented in Table 2.The Ni- and Si-implanted ion profiles were calculated using the Stopping Range of Ions in Materials (SRIM) code [18]. It was found that the Ni- and Si-implanted concentrations at the peak implantation regions are 0.16 and 0.62 at. %, respectively. Table 3 summarizes the calculated values of δ for each phase before and after ion irradiation, taking into account the maximum values of implanted Ni and Si ions and assuming homogenous distributions. It is seen that while the implantation of Ni does not noticeably change δ, Si implantation increases it by 6% and 2% for the A1 and B2 phases, respectively. One reason for this difference is that the atomic size of Ni is nearly equal to most of the HEA constituents (Co, Cr, Fe, Ni), while the atomic size of Si is considerably smaller than all the HEA components.

The response of the A1 and B2 phases to ion irradiation is rather different, according the XRD line broadening and TEM analysis, the

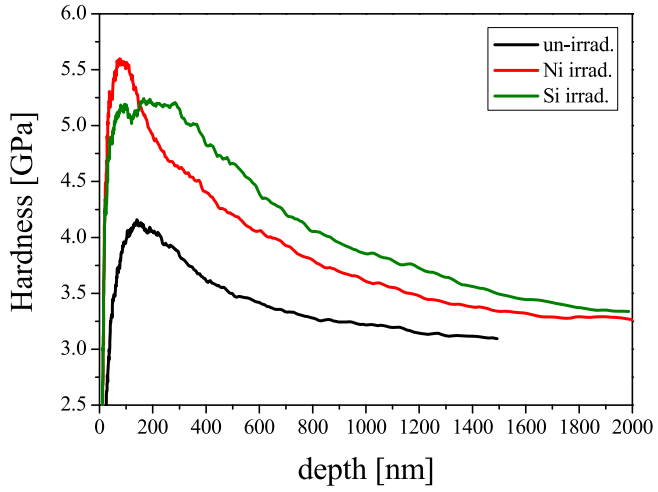

Fig. 6. Nanoindentation results of un-irradiated and ion irradiated $Al_{0.5}$CoCrFeNi alloys following an initial 900 °C heat treatment for 7 days, with irradiations conducted to 18.7 and 15.3 DPA for the cases of Ni and Si ions respectively.

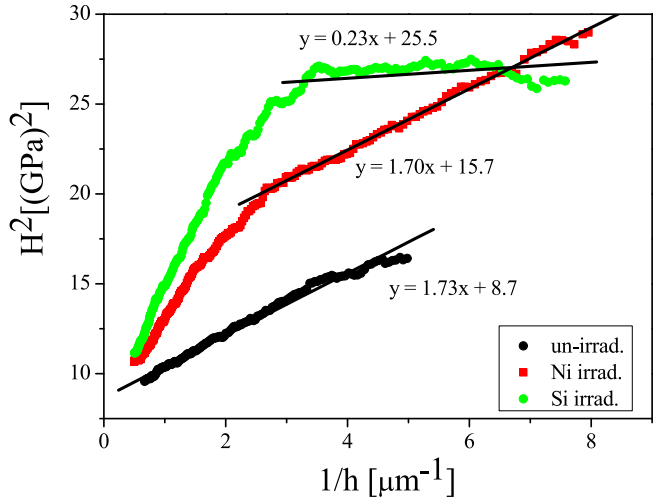

Fig. 7. Nix-Gao plot of nanohardness for ion-irradiated and un-irradiated HEA samples.

Table 1
Calculated nanohardness according the Nix-Gao model.

Sample	H_0 [GPa]	H_0/H_0(un-irradiated)
$Al_{0.5}$CoCrFeNi – Si irradiated, 15.3 dpa	5.05 ± 0.49	1.71
$Al_{0.5}$CoCrFeNi – Ni irradiated, 18.7 dpa	3.96 ± 0.24	1.34
un-irradiated $Al_{0.5}$CoCrFeNi	2.95 ± 0.19	1

Table 2
Composition (at. %) of phases in the $Al_{0.5}$CoCrFeNi alloy after heat treatment at 900 °C as measured by SEM-EDS measurements.

Phase	Al	Co	Cr	Fe	Ni
A1	5.7 ± 0.6	24.8 ± 0.5	27.3 ± 0.5	23.8 ± 0.2	18.4 ± 0.5
B2	35.20.2±	14.3 ± 0.2	5.4 ± 0.15	9.6 ± 0.15	35.5 ± 0.2

response of the B2 phase to irradiation is done by the increase of the elastic strain while in the A1 phase there is an increase of dislocation density and release of strain. This occurs first because the change in δ is much larger for the A1 phase compared to the B2 phase; which drives

Table 3
Calculated values of δ before and after irradiation for A1 and B2 phases.

Phase	Before irradiation	Ni ion irradiation	Si ion irradiation
A1	0.0332	0.0332	0.0352
B2	0.0665	0.0664	0.0680

the A1 phase towards the formation of additional dislocations to accommodate this stress. Second, ordered phases tend to transform to disordered phases under irradiation [38,39] as a direct result of random rearrangement of atoms after Frenkel pair recombination. In the case of the B2 phase, it isn't straightforward since this transformation (from B2 to B1) requires a compositional change [40], which implies a transformation via nucleation and growth mechanism. Furthermore, the deformation mechanism of the B2 phase is via screw dislocations [41]. Feuerbacher [26] studied the deformation behavior in a B2-ordered $Al_{28}Co_{20}Cr_{11}Fe_{15}Ni_{26}$ high-entropy alloy and found that the dislocations in this HEA possess the ⟨111⟩ Burgers vector, which is a full body diagonal of the unit cell and corresponds to a length of 0.50 nm. In terms of the B2 lattice, the dislocations are thus perfect super-dislocations. Feuerbacher also concluded that in the $Al_{28}Co_{20}Cr_{11}Fe_{15}Ni_{26}$ the antiphase boundaries energies (an antiphase boundary separates two domains of the same ordered phase) are very high, which requires significant deformation. In the case of the A1 phase, since it is ductile [41], the damage could be easily compensated by the formation of dislocations. The different response of the A1 and B2 phases to ion irradiation can explain the results of Xia et al. [42], which show that hardening under irradiation increases as the Al content in the Al_xCoCrFeNi alloy increases from 0.1 to 0.75 and 1.75 and the structure is FCC, mixing of FCC and BCC, and BCC, respectively. This finding implies that at room temperature, the susceptibility of the B1 phase to irradiation damage is higher than the A1 phase. Therefore, it is reasonable that at much higher doses, that B2 phase will not be able to maintain internal stresses, and a different deformation mechanism will take place. Nonetheless, the role of dislocations in irradiation hardening of HEAs is significant, for example; Jin et al. [43] studied ion irradiation of Ni-containing equiatomic alloys and came to the conclusion that the primary hardening source may be dislocation (loops). Wang et al. [44] studied the irradiation resistance of the CoCrFeCuNi alloy. They showed that HEAs exhibit marked hardening behavior, which was attributed to obstacles to dislocation glide. They concluded that in general, irradiation-induced defect clusters and/or dislocation loops as well as He bubbles pin dislocation lines and impede dislocation glide, causing HEAs to harden. Lu et al. [45] studied the ion irradiation behavior of the NiCoFeCrMn alloy and concluded that the source of hardening is dislocation loops.

We note that there is still much compositional and phase space to explore even in the Al_xCoCrFeNi HEA system. Our study reveals that there is still room to expand our knowledge and optimize resistance to irradiation, and that the type of radiation applied certainly affects the key results of intrinsic lattice strain in each phase primary thought to be responsible for frustrating 1D defect motion and imparting radiation damage stability. The interplay between the two mechanisms, one at the atomistic level (best highlighted in the $Al_{0.1}$CoCrFeNi HEA) of PEL heterogeneity, one at the microstructural level (best highlighted by our $Al_{0.5}$CoCrFeNi HEA) of high interface density, could be further explored and optimized to minimize defect formation as evidenced by fewer material property changes under irradiation.

Nanohardness, XRD-measured lattice strain, and TEM evidence are all convenient and descriptive measures of radiation resistance. These are all subsets of the overall approach of *minimal material property changes* as the fastest and most comprehensive way to quantify radiation damage resistance. As the same radiation defects and their movement/clustering underpin all the material property changes resultant from radiation damage, there exist links between what may be viewed as disparate material property measures. The playing field then opens up to

monitor changes in thermal and elastic properties as correlated to those mechanical ones of ultimate interest, which in turn suggests the use of faster, *in situ* techniques as the best way to explore the nearly infinite compositional space of potentially radiation-tolerant HEAs. Combining rapid, compositionally perturbative techniques like combinatorial synthesis [46] with similarly rapid, *in situ* methods of thermo-elastic material property evolution [47] may be the most efficient way to search for the "islands of stability" [48] to radiation damage, as has been recently done for similarly compositionally complex optimization like correlating glass formation temperature to antibacterial activity in Zr-Cu-Al-Ag metallic glasses [46], or the discovery of new shape-memory alloys in the Ti-Ni-Cu system [49].

5. Conclusions

We demonstrate the different effects of Si and Ni ion irradiation on the $Al_{0.5}$CoCrFeNi alloy at its equilibrium state. Si ions harden the HEA more on a per-ion basis compared to Ni, and this is attributed to the higher impact on the lattice distortion parameter by Si atoms. It is also demonstrated that the FCC phase and BCC ordered phase respond differently to ion irradiation. Irradiation causes an increase of dislocation density in the FCC phase, while elastic stresses are formed in the ordered BCC phase. This difference is attributed to lattice distortion and deformation mechanism differences between ductile and brittle ordered phases.

Our results also demonstrate that much optimization remains to be performed in HEA systems, and a more concerted, high-throughput effort to search for islands of stability to radiation damage should be conducted to best make use of the nearly infinite compositional possibilities in each HEA system.

CRediT authorship contribution statement

Michael Aizenshtein: Conceptualization, Methodology, Investigation, Formal analysis, Writing - original draft, Writing - review & editing. **Ziv Ungarish:** Methodology, Software, Formal analysis, Investigation, Writing - original draft, Writing - review & editing. **Kevin Woller:** Software, Formal analysis, Investigation, Writing - original draft, Writing - review & editing. **Shmuel Hayun:** Conceptualization, Writing - original draft, Writing - review & editing, Supervision, Funding acquisition. **Michael P. Short:** Methodology, Resources, Writing - original draft, Writing - review & editing, Supervision, Funding acquisition.

Declaration of Competing Interest

The authors declare that they have no known competing financial interests or personal relationships that could have appeared to influence the work reported in this paper.

Acknowledgments

M.P.S. acknowledges support from the U.S. National Science Foundation's CAREER program, under Grant No. DMR-1654548.

Data Availability Statement

All micrographs, raw XRD scans, nanoindentation results, and other files used in the creation of this manuscript can be found at our GitHub data repository [50].

References

[1] Y.Y. Chen, T. Duval, U.D. Hung, J.W. Yeh, H.C. Shih, Microstructure and electrochemical properties of high entropy alloys—a comparison with type-304 stainless steel, Corros. Sci. 47 (2005) 2257–2279, https://doi.org/10.1016/j.corsci.2004.11.008.

[2] C.W. Tsai, M.H. Tsai, J.W. Yeh, C.C. Yang, Effect of temperature on mechanical properties of Al0.5CoCrCuFeNi wrought alloy, J. Alloys. Compd. 490 (2010) 160–165, https://doi.org/10.1016/j.jallcom.2009.10.088.

[3] C.J. Tong, M.R. Chen, S.K. Chen, J.W. Yeh, T.T. Shun, S.J. Lin, S.Y. Chang, Mechanical performance of the AlxCoCrCuFeNi high-entropy alloy system with multiprincipal elements, Metall. Mater. Trans. A. 36 (2005) 1263–1271, https://doi.org/10.1007/s11661-005-0218-9.

[4] Y. Lu, Y. Dong, S. Guo, L. Jiang, H. Kang, T. Wang, B. Wen, W. Zhijun, J.C. Jie, Z. Cao, H.H. Ruan, L. Tingju, A Promising New Class of High-Temperature Alloys: Eutectic High-Entropy Alloys, Sci. Rep. 4 (2015) 6200, https://doi.org/10.1038/srep06200.

[5] T. Allen, J. Busby, M. Meyer, D. Petti, Materials challenges for nuclear systems, Mater Today Off. 13 (2010) 14–23, https://doi.org/10.1016/S1369-7021(10)70220-0.

[6] S.J. Zinkle, G.S. Was, Materials challenges in nuclear energy, Acta Mater. 61 (2013) 735–758, https://doi.org/10.1016/j.actamat.2012.11.004.

[7] T. Yang, S. Xia, S. Liu, C. Wang, S. Liu, Y. Fang, Y. Zhang, J. Xue, S. Yan, Y. Wang, Precipitation behavior of AlxCoCrFeNi high entropy alloys under ion irradiation, Sci. Rep. 6 (2016) 32146, https://doi.org/10.1038/srep32146.

[8] S. Xia, M.C. Gao, T. Yang, P.K. Liaw, Y. Zhang, Phase stability and microstructures of high entropy alloys ion irradiated to high doses, J. Nucl. Mater. 480 (2016) 100–108, https://doi.org/10.1016/j.jnucmat.2016.08.017.

[9] S.Q. Xia, X. Yang, T.F. Yang, S. Liu, Y. Zhang, Irradiation resistance in AlxCoCrFeNi high entropy alloys, JOM. 67 (2015) 2340–2344, https://doi.org/10.1007/s11837-015-1568-4.

[10] W.R. Wang, W.L. Wang, S.C. Wang, Y.C. Tsai, C.H. Lai, J.W. Yeh, Effects of Al addition on the microstructure and mechanical property of AlxCoCrFeNi high-entropy alloys, Intermetallics 26 (2012) 44–51, https://doi.org/10.1016/j.intermet.2012.03.005.

[11] C. Wang, C.L. Tracy, S. Park, J. Liu, Phase transformations of Al-bearing high entropy alloys AlxCoCrFeNi (x=0, 0.1, 0.3, 0.75, 1.5) at high pressure, Appl. Phys. Lett., 114 (2019) 091902. https://doi.org/10.1063/1.5079868.

[12] J. Wang, H.X. Yang, T. Guo, J. Wang, W.Y. Wang, J.S. Li, Effect of cold rolling on the phase transformation kinetics of an Al0.5CoCrFeNi high-entropy alloy, Entropy 20 (12) (2018) 917, https://doi.org/10.3390/e20120917.

[13] N.A.P.K. Kumar, C. Li, K.J. Leonard, H. Bei, S.J. Zinkle, Microstructural stability and mechanical behavior of FeNiMnCr high entropy alloy under ion irradiation, Acta Mater. 113 (2016) 230–244, https://doi.org/10.1016/j.actamat.2016.05.007.

[14] T. Yang, S. Xia, W. Guo, R. Hu, J.D. Poplawsky, G. Sha, Y. Fang, Z. Yan, C. Wang, C. Li, Y. Zhang, S.J. Zinkle, Y. Wang, Effects of temperature on the irradiation responses of Al0.1CoCrFeNi high entropy alloy, Scr. Mater. (2018) 31–35, https://doi.org/10.1016/j.scriptamat.2017.09.025.

[15] T. Yang, W. Guo, J.D. Poplawsky, D. Li, L. Wang, Y. Li, W. Hu, M.L. Crespillo, Z. Yan, Y. Zhang, Y. Wang, S.J. Zinkle, Structural damage and phase stability of Al0.3CoCrFeNi high entropy alloy under high temperature ion irradiation, Acta Mater. 188 (2020) 1–15, https://doi.org/10.1016/j.actamat.2020.01.060.

[16] B. Kombaiah, K. Jin, H. Bei, P.D. Edmondson, Y. Zhang, Phase stability of single phase Al0.12CrNiFeCo high entropy alloy upon irradiation, Mater. Des. 160 (2018) 1208–1216, https://doi.org/10.1016/j.matdes.2018.11.006.

[17] J.F. Ziegler, M.D. Ziegler, J.P. Biersack, SRIM–the stopping and range of ions in matter (2010), Nucl. Instrum. Methods Phys. Res. Sect. B 268 (2010) 1818–1823, https://doi.org/10.1016/j.nimb.2010.02.091.

[18] R.E. Stoller, M.B. Toloczko, G.S. Was, On the use of SRIM for computing radiation damage exposure, Nucl. Instrum. Methods Phys. Res. Sect. B 310 (2013) 75–80, https://doi.org/10.1016/j.nimb.2013.05.008.

[19] ASTM International. E521-96 Standard Practice for Neutron Radiation Damage Simulation by Charged-Particle Irradiation. West Conshohocken, PA; ASTM International, 1996.

[20] M. Vaidya, S. Trubel, B.S. Murty, G. Wilde, S.V. Divinski, Ni tracer diffusion in CoCrFeNi and CoCrFeMnNi high entropy alloys, J. Alloys Compd. 688 (2016) 994–1001.

[21] G.K. Williamson, W.H. Hall, X-ray line broadening from filed aluminium and wolfram, Acta Metall. 1 (1953) 22–31, https://doi.org/10.1016/0001-6160(53)90006-6.

[22] W.R. Wang, W.L. Wang, J.W. Yeh, Phases, microstructure and mechanical properties of AlxCoCrFeNi high-entropy alloys at elevated temperatures, J. Alloys Comp. 589 (2014) 143–152, https://doi.org/10.1016/j.jallcom.2013.11.084.

[23] C.M. Lin, H.L. Tsai, Evolution of microstructure, hardness, and corrosion properties of high-entropy Al0.5CoCrFeNi alloy, Intermetallics 19 (2011) 288–294, https://doi.org/10.1016/j.intermet.2010.10.008.

[24] M. Aizenshtein, E. Strumza, E. Brosh, S. Hayun, Microstructure, Kinetics and Thermodynamics of the Al0.5CoCrFeNi HEA, manuscript in review.

[25] S. Lee, M.J. Duarte, M. Feuerbacher, R. Soler, C. Kirchlechner, C.H. Liebscher, S. H. Oh, G. Dehm, Dislocation plasticity in FeCoCrMnNi high-entropy alloy: quantitative insights from in-situ transmission electron microscopy deformation, Mater. Res. Lett. 8 (2020) 216–224, https://doi.org/10.1080/21663831.2020.1741469.

[26] M. Feuerbacher, Dislocations and deformation microstructure in a B2-ordered Al28Co20Cr11Fe15Ni26 high-entropy alloy, Sci. Rep. 6 (2016) 29700, https://doi.org/10.1038/srep29700.

[27] S. Sinha, S.S. Nene, M. Frank, K. Liu, P. Agrawal, R.S. Mishra, On the evolving nature of c/a ratio in a hexagonal close-packed epsilon martensite phase in transformative high entropy alloys, Sci. Rep. 9 (2019) 1–14, https://doi.org/10.1038/s41598-019-49904-5.

[28] W.D. Nix, H. Gao, Indentation size effects in crystalline materials: a law for strain gradient plasticity, J. Mech. Phys. Solids 46 (1998) 411–425, https://doi.org/10.1016/S0022-5096(97)00086-0.
[29] M.R. He, S. Wang, S. Shi, K. Jin, H. Bei, K. Yasuda, S. Matsumura, K. Higashida, I. M. Robertson, Mechanisms of radiation-induced segregation in CrFeCoNi-based single-phase concentrated solid solution alloys, Acta Mater. 126 (2017) 182–193, https://doi.org/10.1016/j.actamat.2016.12.046.
[30] W. Chen, X. Ding, Y. Feng, X. Liu, K. Liu, Z. Lu, D. Li, Y. Li, C. Liu, X.-Q. Chen, Vacancy formation enthalpies of high-entropy FeCoCrNi alloy via first-principles calculations and possible implications to its superior radiation tolerance, J. Mater. Sci. Technol. 34 (2018) 355–364, https://doi.org/10.1016/j.jmst.2017.11.005.
[31] M. Jin, P. Cao, M.P. Short, Thermodynamic mixing energy and heterogeneous diffusion uncover the mechanisms of radiation damage reduction in single-phase Ni-Fe alloys, Acta Mater. 147 (2018) 16–23, https://doi.org/10.1016/j.actamat.2017.12.064.
[32] C. Lu, L. Niu, N. Chen, K. Jin, T. Yang, P. Xiu, Y. Zhang, F. Gao, H. Bei, S. Shi, et al., Enhancing radiation tolerance by controlling defect mobility and migration pathways in multicomponent single-phase alloys, Nat. Commun. 7 (2016) 13564, https://doi.org/10.1038/ncomms13564.
[33] F. Granberg, K. Nordlund, M.W. Ullah, K. Jin, C. Lu, H. Bei, L.-M. Wang, F. Djurabekova, W.J. Weber, Y. Zhang, Mechanism of radiation damage reduction in equiatomic multicomponent single-phase alloys, Phys. Rev. Lett. 116 (2016) 135504–135509, https://doi.org/10.1103/PhysRevLett.116.135504.
[34] Z. Wang, C.T. Liu, P. Dou, Thermodynamics of vacancies and clusters in high-entropy alloys, Phys. Rev. Mater. 1 (2017), https://doi.org/10.1103/PhysRevMaterials.1.043601.
[35] J.W. Qiao, S.G. Ma, E.W. Huang, C.P. Chuang, P.K. Liaw, Y. Zhang, Microstructural characteristics and mechanical behaviors of AlCoCrFeNi high-entropy alloys at ambient and cryogenic temperatures, Mater. Sci. Forum 688 (2011) 419–425.
[36] Y. Zhang, Y.J. Zhou, J.P. Lin, G.L. Chen, P.K. Liaw, Solid-solution phase formation rules for multi-component alloys, Adv. Eng. Mater. 10 (2008) 534–538, https://doi.org/10.1002/adem.200700240.
[37] A.F. Wells, Structural Inorganic Chemistry, fifth ed., Clarendon Press Oxford, London 1984.
[38] K.Y. Liou, P. Wilkes, The radiation disorder model of phase stability, J. Nucl. Mater. 87 (1979) 317–330, https://doi.org/10.1016/0022-3115(79)90568-3.
[39] K.C. Russell, Phase Stability under Irradiation, Prog. Mater. Sci. 28 (1985) 229–434, https://doi.org/10.1016/0079-6425(84)90001-X.
[40] M. Aizenshtein, E. Strumza, E. Brosh, S. Hayun, Precipitation Kinetics, Microstructure and Equilibrium state of the A2 and B2 phases in the Multi Component Al2.75CoCrFeNi Alloy, J. Mater. Sci. 55 (2020) 7016–7028, https://doi.org/10.1007/s10853-020-04487-9.
[41] M. Yamaguchi, Y. Umakoshi, The deformation behaviour of intermetallic superlattice Compounds, Prog. Mat. Sci. 34 (1990) 1–148, https://doi.org/10.1016/0079-6425(90)90002-Q.
[42] S.-Q. Xia, Z. Wang, T.-F. Yang, Y. Zhang, Irradiation behavior in high entropy alloys, J. Iron Steel Res. Intl. 22 (2015) 879–884, https://doi.org/10.1016/S1006-706X(15)30084-4.
[43] K. Jin, C. Lu, L.M. Wang, J. Qu, W.J. Weber, Y. Zhang, H. Bei, Effects of compositional complexity on the ion-irradiation induced swelling and hardening in Ni-containing equiatomic alloys, Scripta Mater. 119 (2016) 65–70, https://doi.org/10.1016/j.scriptamat.2016.03.030.
[44] Y. Wang, K. Zhang, Y. Feng, Y. Li, W. Tang, B. Wei, Evaluation of radiation response in CoCrFeCuNi high-entropy alloys, Entropy 20 (2018) 835–847, https://doi.org/10.3390/e20110835.
[45] C. Lu, T. Yang, K. Jin, N. Gao, P. Xiu, Y. Zhang, F. Gao, H. Bei, W.J. Weber, K. Sun, Y. Dong, L. Wang, Radiation-induced segregation on defect clusters in single-phase concentrated solid-solution alloys, Acta Mater. 127 (2017) 98–107, https://doi.org/10.1016/j.actamat.2017.01.019.
[46] Y. Liu, J. Padmanabhan, B. Cheung, J. Liu, Z. Chen, B.E. Scanley, D. Wesolowski, M. Pressley, C.C. Broadbridge, S. Altman, U.D. Schwarz, T.R. Kyriakides, J. Schroers, Combinatorial development of antibacterial Zr-Cu-Al-Ag thin film metallic glasses, Sci. Rep. 6 (2016) 26950, https://doi.org/10.1038/srep26950.
[47] F. Hofmann, M.P. Short, C.A. Dennett, Transient grating spectroscopy: An ultrarapid, nondestructive materials evaluation technique, MRS-B 44 (2019) 392–402, https://doi.org/10.1557/mrs.2019.104.
[48] G. Giannopoulos, G. Barucca, A. Kaidatzis, V. Psycharis, R. Salikhov, M. Farle, E. Koutsoufakis, D. Niarchos, A. Mehta, M. Scuderi, et al. L10-FeNi films on Au-Cu-Ni buffer-layer: a high-throughput combinatorial study, Sci. Rep. 8 (2018) 15919, https://doi.org/10.1038/s41598-018-34296-9.
[49] R. Zarnetta, D. König, C. Zamponi, A. Aghajani, J. Frenzel, G. Eggeler, A. Ludwig, R-phase formation in Ti39Ni45Cu16 shape memory thin films and bulk alloys discovered by combinatorial methods, Acta Mater. 57 (2009) 4169–4177, https://doi.org/10.1016/j.actamat.2009.05.014.
[50] GitHub repository for this manuscript, available at https://github.com/shortlab/2020-Aizenshtein-HEAs.